BJP British Journal of Pharmacology

DOI:10.1111/bph.12838
www.brjpharmacol.org

RESEARCH PAPER

Celastrol protects ischaemic myocardium through a heat shock response with up-regulation of haeme oxygenase-1

Correspondence
Dr Nicolas Noiseux, Centre Hospitalier de l'Université de Montréal (CHUM), 3840 Saint-Urbain Street, Montreal, QC, Canada, H2W1T8. E-mail: noiseuxn@videotron.ca

Received
2 December 2013
Revised
12 May 2014
Accepted
1 July 2014

S Der Sarkissian[1,2], J-F Cailhier[1,3,4], M Borie[1], L-M Stevens[1,2], L Gaboury[3,5], S Mansour[1,3], P Hamet[1,3] and N Noiseux[1,2]

[1]*Centre de Recherche du Centre Hospitalier de l'Université de Montréal (CRCHUM), Montreal, Quebec, Canada, Departments of* [2]*Surgery and* [3]*Medicine, Faculty of Medicine, and* [5]*Institute for Research in Immunology and Cancer, Université de Montréal, Montreal, Quebec, Canada,* [4]*Montreal Cancer Institute, Montreal, Quebec, Canada*

BACKGROUND AND PURPOSE

Celastrol, a triterpene from plants, has been used in traditional oriental medicine to treat various diseases. Here, we investigated the cardioprotective effects of celastrol against ischaemia.

EXPERIMENTAL APPROACH

Protective pathways induced by celastrol were investigated in hypoxic cultures of H9c2 rat cardiomyoblasts and in a rat model of myocardial infarction, assessed with echocardiographic and histological analysis.

KEY RESULTS

In H9c2 cells, celastrol triggered reactive oxygen species (ROS) formation within minutes, induced nuclear translocation of the transcription factor heat shock factor 1 (HSF1) resulting in a heat shock response (HSR) leading to increased expression of heat shock proteins (HSPs). ROS scavenger N-acetylcysteine reduced expression of HSP70 and HSP32 (haeme oxygenase-1, HO-1). Celastrol improved H9c2 survival under hypoxic stress, and functional analysis revealed HSF1 and HO-1 as key effectors of the HSR, induced by celastrol, in promoting cytoprotection. In the rat ischaemic myocardium, celastrol treatment improved cardiac function and reduced adverse left ventricular remodelling at 14 days. Celastrol triggered expression of cardioprotective HO-1 and inhibited fibrosis and infarct size. In the peri-infarct area, celastrol reduced myofibroblast and macrophage infiltration, while attenuating up-regulation of TGF-β and collagen genes.

CONCLUSIONS AND IMPLICATIONS

Celastrol treatment induced an HSR through activation of HSF1 with up-regulation of HO-1 as the key effector, promoting cardiomyocyte survival, reduction of injury and adverse remodelling with preservation of cardiac function. Celastrol may represent a novel potent pharmacological cardioprotective agent mimicking ischaemic conditioning that could have a valuable impact in the treatment of myocardial infarction.

Abbreviations

ALT, alanine transaminase; AST, aspartate aminotransferase; EDD, end-diastolic diameter; EDV, end-diastolic volume; ESD, end-systolic diameter; ESV, end-systolic volume; GGT, γ-glutamyl transpeptidase; HO-1, haeme oxygenase-1; HPS, haematoxylin phloxine saffron; HSF1, heat shock factor 1; HSPs, heat shock proteins; HSR, heat shock response; LV, left ventricular; LVAW, left ventricular anterior wall; LVEF, left ventricular ejection fraction; LVFS, left ventricular fractional shortening; MI, myocardial infarction; NAC, N-acetylcysteine; ROS, reactive oxygen species; SV, stroke volume; TNT, troponin T; ZnPP-9, zinc protoporphyrin-9

Table of Links

TARGETS	LIGANDS
Collagen I	PD98059
Collagen III	TGF-β3
HO-1, haeme oxygenase 1	Wortmannin
HSP90, heat shock protein 90	

This Table lists key protein targets and ligands in this article which are hyperlinked to corresponding entries in http://www.guidetopharmacology.org, the common portal for data from the IUPHAR/BPS Guide to PHARMACOLOGY (Pawson *et al.*, 2014) and are permanently archived in the Concise Guide to PHARMACOLOGY 2013/14 (Alexander *et al.*, 2013).

Introduction

Ischaemic cardiac disease is a leading cause of morbidity and mortality (Finegold *et al.*, 2013). While reperfusion therapies aim to reduce infarct size, reperfusion alone cannot eliminate irreversible damages caused by myocardial infarction (MI), so muscle lost is replaced by non-contractile fibrotic scar tissue (Laflamme *et al.*, 2007). Any intervention preserving the viability of ischaemic myocardium will reduce infarct size and improve repair, thus decreasing the risk of developing heart failure or death (Solomon *et al.*, 2005).

Ischaemic conditioning, with brief sublethal ischaemic episodes followed by reperfusion, is a cardioprotective mechanism that promotes expression of survival signals protecting the heart from subsequent ischaemic insult and limits MI size (Murry *et al.*, 1991). Conditioning treatments can be administered before (pre-conditioning), immediately after the onset of MI (post-conditioning) or remotely with the same protective effects (Ovize *et al.*, 2013). Likewise, thermal conditioning (heat shock) also confers cellular resistance and derives its benefits from activation of heat shock proteins (HSPs). HSPs are molecular chaperones that govern the proper folding of newly synthesized proteins, enhance the ability of stressed cells to cope with increased concentrations of denatured proteins, and are responsible for cellular survival and anti-apoptotic signalling (Haider and Ashraf, 2008). Pharmacological agents mimicking ischaemic or thermal conditioning are being actively investigated, and in that effort, we identified celastrol as a potent inducer of the heat shock response (HSR) and survival signals.

Celastrol, a triterpene originally extracted from the root bark of a traditional oriental medicinal plant the 'thunder god vine' (*Tripterygium wilfordii* Hook F.) is recognized as one of the most promising medicinal molecules isolated from plant extracts (Salminen *et al.*, 2010). Celastrol has demonstrated beneficial effects in the treatment of different forms of neurodegenerative, autoimmune and inflammatory diseases (Salminen *et al.*, 2010). In this study, celastrol was investigated for the treatment of ischaemic myocardium, by characterizing its cytoprotective properties and deciphering the activation of survival signalling pathways. This is the first report presenting the cardioprotective effects of celastrol in the context of ischaemic heart disease. The results suggest that celastrol treatment of cardiomyocytes through the HSR and up-regulation of haeme oxygenase-1 (HO-1) could represent a novel pharmacological 'conditioning mimetic' that can be used for the treatment of ischaemic heart to reduce infarct size and improve repair.

Methods

In vitro *studies*

Cell culture and in vitro *treatments.* Rat cardiomyoblast H9c2 cells [H9C2(2-1), American Type Culture Collection (Manassas, VA, USA)] were cultured at 37°C in media (DMEM high glucose, Life Technologies, Burlington, ON, Canada) supplemented with 10% FBS (Life Technologies). Cells were treated with the same media supplemented with 1% FBS and containing either celastrol (10^{-10} – 10^{-6} M; Cayman Chemical, Ann Arbor, MI, USA) or its vehicle (DMSO: 0.1% v/v, Sigma-Aldrich, Oakville, ON, Canada). For signalling pathway investigations, cells were pretreated for 3 h with the following inhibitors: wortmannin (PI3K/Akt inhibitor; 1 μM, Calbiochem, Etobicoke, ON, Canada), PD98059 (MAPK/ERK inhibitor; 50 μM, Calbiochem), N-acetylcysteine (NAC: 2.5 mM, Sigma-Aldrich), Kribb11 [heat shock factor 1, HSF1 inhibitor (Yoon *et al.*, 2011); 7.5 μM, Calbiochem] and zinc protoporphyrin-9 (ZnPP-9: HO-1 activity inhibitor; 100 nM, Calbiochem), and maintained in media containing low concentrations of inhibitors (wortmannin, 100 nM; PD98059, 5 μM; NAC, 156 μM; Kribb11, 100 nM; ZnPP-9. 10 nM) until processing for viability studies.

Protein and mRNA expression. Expression studies were conducted as previously described (Noiseux *et al.*, 2012). Equal concentrations of proteins were probed by Western blot using the following antigens: total and phospho-Akt (Cell Signaling, Danvers, MA, USA), total and phospho-ERK1/2 (Cell Signaling), HO-1 (HSP32; Enzo Life Sciences), HSP70 (Enzo Life Sciences, Farmingdale, NY, USA), α-smooth muscle actin [αSMA; anti-actin α-smooth muscle antibody (Clone 1A4), Sigma-Aldrich] and anti-GAPDH (Sigma-Aldrich). For HSF1 (Enzo Life Sciences) detection, proteins were isolated from nuclear and cytoplasmic extracts similarly as described (Schett *et al.*, 1999), and protein content was normalized with anti-GAPDH antibody for the cytoplasmic extract and anti-transcription factor II D antibody (Santa Cruz, Dallas, TX, USA) for the nuclear fraction. Autoradiographs were quantified by densitometric scanning (Quantity One software, Bio-Rad).

Messenger RNA expression of selected genes was characterized by semi-quantitative real-time RT-PCR with specific primer sequences (Supporting Information) and Sybr Green Real-Time PCR kit (Life Technologies) according to the manufacturer's protocol. The 18S gene was used as endogenous control, and results are expressed as fold changes and compared with control untreated cultures according to the Pfaffl method (Pfaffl, 2001).

Reactive oxygen species (ROS) measurement. H9c2 cells were incubated for 60 min with 10 μM CM-H2DCFDA (Life Technologies) resuspended in DMEM without phenol (Life Technologies) in low serum, washed once in PBS and stimulated with either vehicle (DMSO) or celastrol. ROS production was measured by fluorescence acquisition using a microplate reader (Victor 3V, Perkin Elmer, Waltham, MA, USA).

Viability assay. H9c2 cell death was induced in DMEM low glucose (Life Technologies) with serum starvation and hypoxic culture condition (<1% O_2) in hypoxia chambers as previously described (Noiseux *et al.*, 2012). H9c2 were cultured and treated with pathway inhibitors, followed by treatment with celastrol as described above. After 48 h, cell viability was assessed with the LIVE/DEAD Viability kit (Life Technologies) according to the manufacturer's protocol. Digital pictures were taken from a fluorescent microscope (IX71, Olympus, Center Valley, PA, USA), and results were quantified using ImageJ software (http://rsbweb.nih.gov/ij/).

In vivo *studies*

MI. All animal care and experimental protocols conformed to the Guide for the Care and Use of Laboratory Animals and were approved by the institutional animal care and use committee of the CHUM Research Center. All studies involving animals are reported in accordance with the ARRIVE guidelines for reporting experiments involving animals (Kilkenny *et al.*, 2010; McGrath *et al.*, 2010).

Thirty-one Sprague-Dawley rats all female (7–8-week-old; CD CRL, Charles River, Senneville, QC, Canada) receiving food and water *ad libitum* were anaesthetized with 2–4% isoflurane (Abbott, Abbott Park, IL, USA) in 1 L·min^{-1} of oxygen. Bupivacaine (2 mg·kg^{-1} s.c.) was injected at the site of the chest incision and through a left parasternal incision, MI was performed by a permanent occlusion of the left anterior descending coronary artery at 4–5 mm from the tip of the left auricle as described and blanching of the tissue confirmed infarct (Noiseux *et al.*, 2006). The suture was not ligated in sham-operated animals, the chest cavity was closed, and animals were extubated when spontaneous respiration resumed (Der Sarkissian *et al.*, 2008). All animals received warm saline 5 mL·kg^{-1} i.p., buprenorphine hydrochloride (0.05 mg·kg^{-1} s.c. daily), carprophen (5 mg·kg^{-1} s.c., daily for 2 days) and rats were closely monitored for vital signs and signs of discomfort throughout the study.

Animal treatments. Myocardial infarcted and sham-operated animals were randomly assigned to either vehicle or celastrol group. Celastrol was administered at a dose of 1 mg·kg^{-1} i.p. daily for 14 days, with the treatment initiated within 3 h following recovery from surgery. Experimental groups were (i) sham surgery + vehicle (control sham, n = 6); (ii) sham surgery + celastrol (treated sham, n = 7); (iii) ligation surgery + vehicle (control ischaemia, n = 10); and (iv) ligation surgery + celastrol (treated ischaemia, n = 8). All animals survived the surgical procedure and treatments. A separate group of rats was injected i.p. with vehicle (n = 8) or celastrol (n = 8) as described earlier without any surgical procedure for measurement of cardiac protein expression after 12 h of treatment and plasma concentration of HO-1 (1:2 dilution, EIA kit, Enzo Life Sciences). In a pilot toxicity screening experiment, another group of rats received saline (0.9% NaCl; n = 3), vehicle (DMSO; n = 3) or celastrol (n = 4, 1 mg·kg^{-1} i.p.) daily for 14 days without any surgical procedure. Serum was collected and analysed using the ADVIA 1800 analyser (Siemens, Munich, Germany) for general markers useful in monitoring health and safety of treatments [uric acid, creatinine, aspartate aminotransferase (AST), alanine transaminase (ALT), γ-glutamyl transpeptidase (GGT), high-sensitivity troponin T (TNT)] (Supporting Information). After 14 days, the rats were killed, and the hearts, livers and kidneys were collected, processed, and stained with standard histological protocols for analysis by a pathologist (not shown).

Cardiac function assessment. Baseline (pretreatment) and 2 week echocardiographic assessments of left ventricular (LV) anatomy and function were performed under 2% isoflurane anaesthesia as previously described (Aceros *et al.*, 2011; Stabile *et al.*, 2011) using a Sonos 5500 Imaging System (Philips, Philips Healthcare, Andover, MA, USA) with a 12 MHz transducer. An M-mode tracing of the LV cavity allowed measurements of LV end-diastolic and end-systolic diameters (EDD and ESD respectively). Percentage of LV fractional shortening (LVFS) was calculated as: $\%LVFS = (EDD - ESD)/EDD \times 100$. LV end-diastolic volume (EDV) and end-systolic volume (ESV) were calculated according to Teichholz method: $[7 \times ESD^3/(2.4 + ESD)]$ and $[7 \times EDD^3/(2.4 + EDD)]$. Percentage of LV ejection fraction (LVEF) was calculated as $\%LVEF = (SV/EDV) \times 100$ where SV is the stroke volume ($EDV - ESV$), and LV anterior wall (LVAW) measurements were collected. All measures were acquired by the same experienced observer, blinded to the treatment. For each measurement, three to five representative cardiac cycles were analysed and averaged.

Tissue collection and histological analysis. After 2 weeks of treatment, animals were anaesthetized with pentobarbital sodium (75 mg·kg^{-1} i.p.), exsanguinated by perfusion with normal saline supplemented with 40 mM KCl and hearts were rapidly removed. Thick (2–3 mm) axial cross sections of the LV immediately distal to the ligation were fixed in 10% formalin and processed for paraffin embedding. The remaining tissues were dissected according to infarct border and remote viable regions of the LV and snap frozen in liquid nitrogen for gene and protein expression studies.

Fibrotic area was evaluated on heart tissue sections stained with Masson's trichrome as described previously (Noiseux *et al.*, 2006; Nguyen *et al.*, 2010). Digitized pictures were analysed by planimetry, and fibrosis was expressed as percentage of stained area over total LV. Macrophage infiltration was determined in ventricular cross sections stained with macrophage F4/80 antibody (Thermo Fisher Scientific, Ottawa, ON, Canada) with kits from Vector (Burlington, ON,

Canada) (secondary antibody, the ABC kit followed by the DAB kit). For each rat, all macrophages in five random pictures in the peri-infarct area were counted, and results were averaged and expressed as macrophages per field.

Finally, global cardiac damage index and all other histological scoring of tissue sections were generated by a pathologist unaware of the experimental treatment groups. Briefly, for the global cardiac damage index score, sections were given a score from 0 (absent) to 4 (high) for the following histopathological phenotypes measured in the infarct area: αSMA content provided separately by blood vessels indicative of neovascularization and by tissue indicative of myofibroblast infiltration, fibrosis by Masson's trichrome stain, collagen and elastin content by Verhoeff stain, and macrophage infiltration by anti-CD68 antibody (ED1) stain. Scores were added and results expressed as a global damage index.

Data analysis

Data are expressed as mean ± SE or median with interquartile range. Groups were compared using ANOVA with Tukey's correction for multiple comparisons (or Dunnett's correction if groups were only compared with control) or Kruskal–Wallis with Dunn's correction, as appropriate. For repeated measurements, paired *t*-tests or linear mixed-effect models were used to compare groups (MIXED procedures in SAS software, version 9.2; SAS Institute, Cary, NC, USA). Between-group differences were assessed. Macrophage infiltration was analysed by unpaired *t*-test. For all analyses, $P < 0.05$ was considered statistically significant.

Results

Celastrol activates PI3K/Akt, ERK1/2 pathways dependent on ROS signalling

Preliminary experiments using celastrol in various cell types ranging from 10^{-10} to 5×10^{-6} M showed rapid activation of intracellular pathways, superior maintenance of cell viability and peak expression of cytoprotective genes at 10^{-6} M dose for 60 min (not shown). The 10^{-6} M dose was selected for use in all *in vitro* experiments. Celastrol treatment rapidly and significantly increased ROS production in H9c2 cells compared with untreated cells ($P = 0.002$ repeated measurements) (Figure 1A). Celastrol demonstrated activation of kinase pathways with peak increase of phosphorylated Akt over total Akt and phosphorylated ERK/total ERK compared with control untreated H9c2 cells after 30 and 15 min respectively (not shown). The observation that the celastrol-induced phosphorylations were sensitive to wortmannin (PI3K/Akt inhibitor), PD98059 (ERK1/2 inhibitor) and the ROS scavenger NAC demonstrated the role of ROS in mediating celastrol-induced pathway activations (Figure 1B, C).

Celastrol induces a HSR: Implication of HSF1 transcription factor and ROS

A 60–120 min treatment of H9c2 cells with celastrol induced the translocation of HSF1 protein from the cytoplasm to the nuclear fraction indicative of its activation (Figure 2A). RT-PCR highlighted a significant (all $P < 0.001$) increase in HSP27 (3.6 ± 0.9-fold), HSP32 (HO-1, 9.3 ± 2.0-fold), HSP60 (3.1 ± 0.5-fold), HSP70 (14.4 ± 3-fold), HSP90a1 (HSP90α) (2.7 ± 0.4-fold), HSP90ab1 (HSP90β) (2.4 ± 0.2-fold), HSP105 (3.7 ± 0.8-fold) and VEGFa (1.6 ± 0.1-fold) mRNA expression in H9c2 cultures treated with 10^{-6} M celastrol for 60 min followed by 3 h washout compared with controls (Figure 2B). When submitted to hypoxia after treatment, control-treated H9c2 showed no change in HSP expression, but a significant 1.7-fold increase ($P = 0.003$) in VEGF mRNA. However, celastrol-treated cells in hypoxia showed further increased mRNA expression for HSP32 (HO-1: 1.9-fold) and VEGF (1.7-fold) compared with normoxic celastrol-treated cells (not shown).

To confirm the presence of key HSPs at the protein level, following a 60 min stimulation with celastrol and a washout period extending until 24 h, significant peak increases of 2.5 ± 0.3-fold for HSP70 ($P = 0.002$), 4.7 ± 0.9-fold for HSP32 (HO-1: $P < 0.001$) and 1.3 ± 0.2-fold for HSP27 ($P = 0.023$) expressions were observed compared with controls at 3 and 6 h following celastrol treatment (Figure 2C).

The role of ROS and HSF1 signalling in the expression of major HSPs were investigated with pathway inhibitors: PI3K/Akt (wortmannin,); ERK1/2 (PD98059); ROS scavenger (NAC); and HSF1 inhibitor (Kribb11). Celastrol significantly increased the protein expression of HSP70 and HSP32 ($P <$ 0.001 vs. controls) (Figure 2D). Kribb11 and NAC blocked the celastrol-increased expression of HSP70 and HSP32, but no change was observed with wortmannin or PD98059 (Figure 2D). This suggests the importance of HSF1 activation and ROS generation in the up-regulation of HSP70 and HSP32.

Celastrol improves cell viability under hypoxia

Celastrol concentration-dependently prevented cell death in H9c2 exposed to hypoxia for 48 h (control: 29.4 ± 3.9% vs. celastrol 10^{-6} M: 17.4 ± 1.2%, $P = 0.01$) (Figure 3A, B). To determine the signalling pathways involved in celastrol-induced survival, experiments were repeated with celastrol (10^{-6} M) and corresponding inhibitors. The use of Kribb11 and HO-1 activity inhibitor (ZnPP-9) significantly prevented survival in celastrol-treated cells, demonstrating the important role of HSF1 and HO-1 signalling in the improved viability after celastrol (Figure 3C).

In vivo *daily celastrol treatment is well tolerated*

In vivo daily celastrol treatment (1 mg·kg^{-1}, i.p.) continuously for 14 days was well tolerated without any adverse events observed. Biochemical analyses of plasma samples at days 1, 3, 7 and 14 showed no difference in uric acid, creatinine, AST, ALT, GGT, TNT levels among all the treatment groups (saline, vehicle (DMSO) or celastrol) (Supporting Information). Moreover, histopathological analysis of the heart, liver and kidneys of these rats showed no tissue damage or injury after 14 days of treatment (not shown).

Up-regulation of HO-1 protein expression in the heart following systemic administration of celastrol

Twelve hours following a single i.p. celastrol (1 mg·kg^{-1}) injection, up-regulation of cardioprotective proteins were

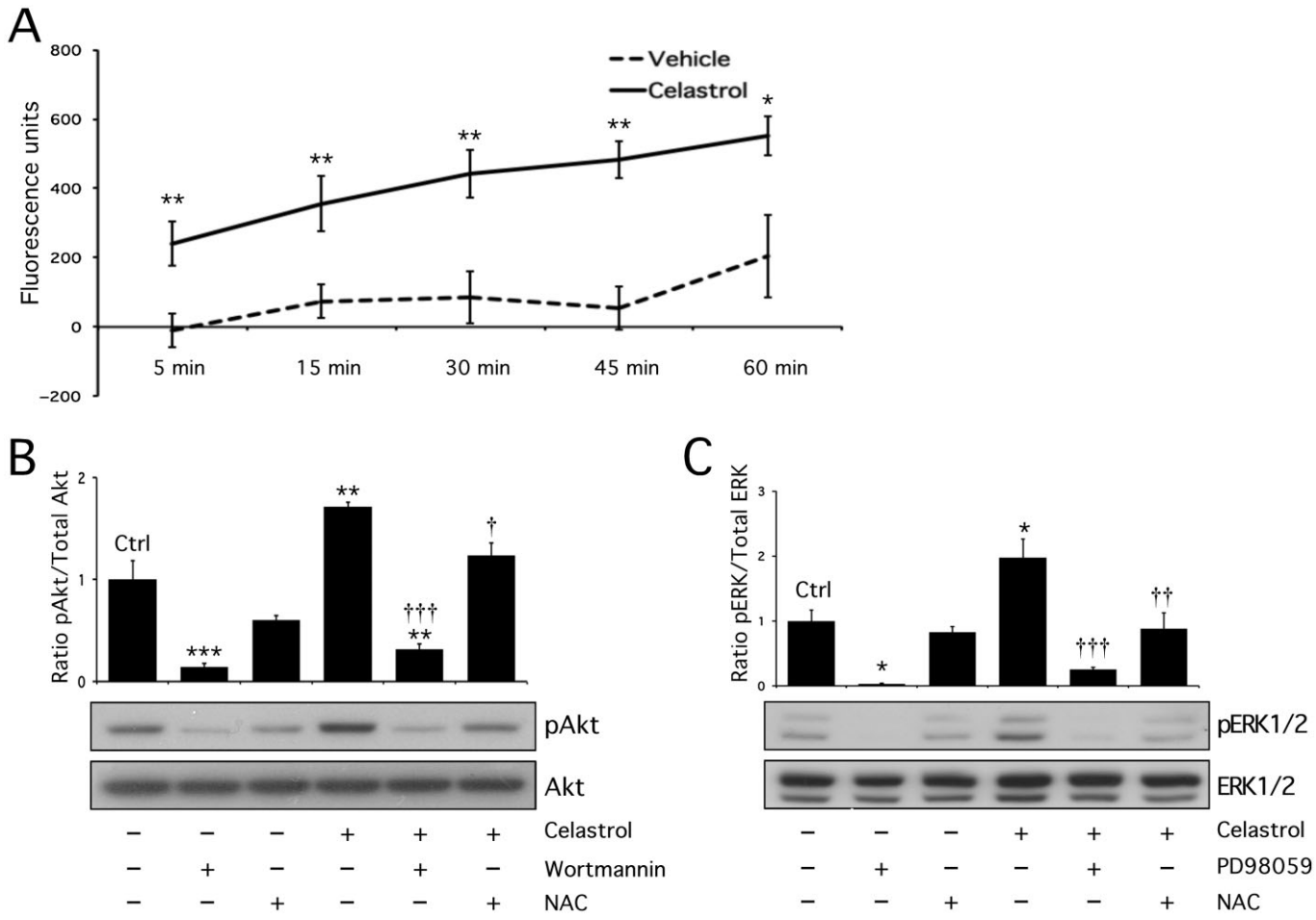

Figure 1

Celastrol activates PI3K/Akt and ERK1/2 pathways in H9c2 cultures dependent on ROS signalling. (A) ROS production was significantly increased 5–60 min after celastrol treatment compared with vehicle-treated H9c2 ($P = 0.002$ repeated measurements). Celastrol's peak activation of (B) pAkt/total Akt (30 min) and (C) pERK/total ERK (15 min) pathways is blocked by the corresponding inhibitors (wortmannin and PD98059) and NAC (ROS scavenger). pAkt, phosphorylated Akt; pERK, phosphorylated ERK. *$P < 0.05$, **$P < 0.01$ and ***$P < 0.001$ versus control or vehicle respectively. †$P < 0.05$, ††$P < 0.01$ and †††$P < 0.001$ versus celastrol in celastrol-treated cells.

detected in the heart of treated rats ($n = 8$) with overexpression of HSP32 (HO-1) compared with controls ($n = 8$) ($P < 0.0001$, Figure 4). Moreover, celastrol increased plasma concentration of HO-1 protein by 4.5-fold (control: 0.52 ± 0.06 ng·mL^{-1} vs. celastrol: 2.33 ± 0.93 ng·mL^{-1}, $P = 0.05$).

Celastrol reduces infarct and prevents adverse remodelling in ischaemic rat myocardium

Coronary artery occlusion resulted in a relatively large infarct as demonstrated by planimetric quantification of Masson's trichrome staining at the papillary muscle level (control ischaemia: 23.9 ± 2.2% vs. control sham 2.1 ± 0.4% and treated sham 1.7 ± 0.3%; $P < 0.001$) (Figure 5A, B). Celastrol treatment significantly reduced adverse remodelling as evaluated by the presence of fibrosis in infarcted hearts by almost 50% (treated ischaemia: 13.0 ± 1.2% vs. control ischaemia: 23.9 ± 2.2%; $P < 0.001$) (Figure 5A, B). Densitometric quantification of αSMA protein by Western blots of extracts of sham-treated hearts showed no difference with treatment (control sham: 0.30 ± 0.08 vs. treated sham: 0.31 ± 0.11; not significant). However, infarct border zone tissues showed a sevenfold increase in αSMA content in control ischaemia hearts, and a 37% significant attenuation with celastrol treatment (control ischaemia: 2.05 ± 0.25 vs. treated ischaemia: 1.18 ± 0.23; $P = 0.017$) (Figure 5C).

As αSMA is representative of myofibroblast infiltration (Santiago *et al.*, 2010), but is also expressed in vascular walls, we analysed αSMA expressed by blood vessels and myofibroblasts, separately, by high-resolution photographs (Figure 5D). Analyses for blood vessel walls revealed no change in vascular αSMA in the infarct border zones of celastrol versus vehicle-treated ischaemic rat hearts ($n = 5$–6, Figure 5E). Moreover, a separate scoring of a subgroup of haematoxylin phloxine saffron (HPS)-stained heart tissue sections by a pathologist showed no difference in blood vessel density ($n = 5$–6 animals) in the infarct border zones in celastrol- or vehicle-treated ischaemic rat hearts (not shown).

However, αSMA of myofibroblast origin in ischaemic tissue was significantly reduced by celastrol treatment ($P < 0.05$) demonstrating a significant reduction in myofibroblast

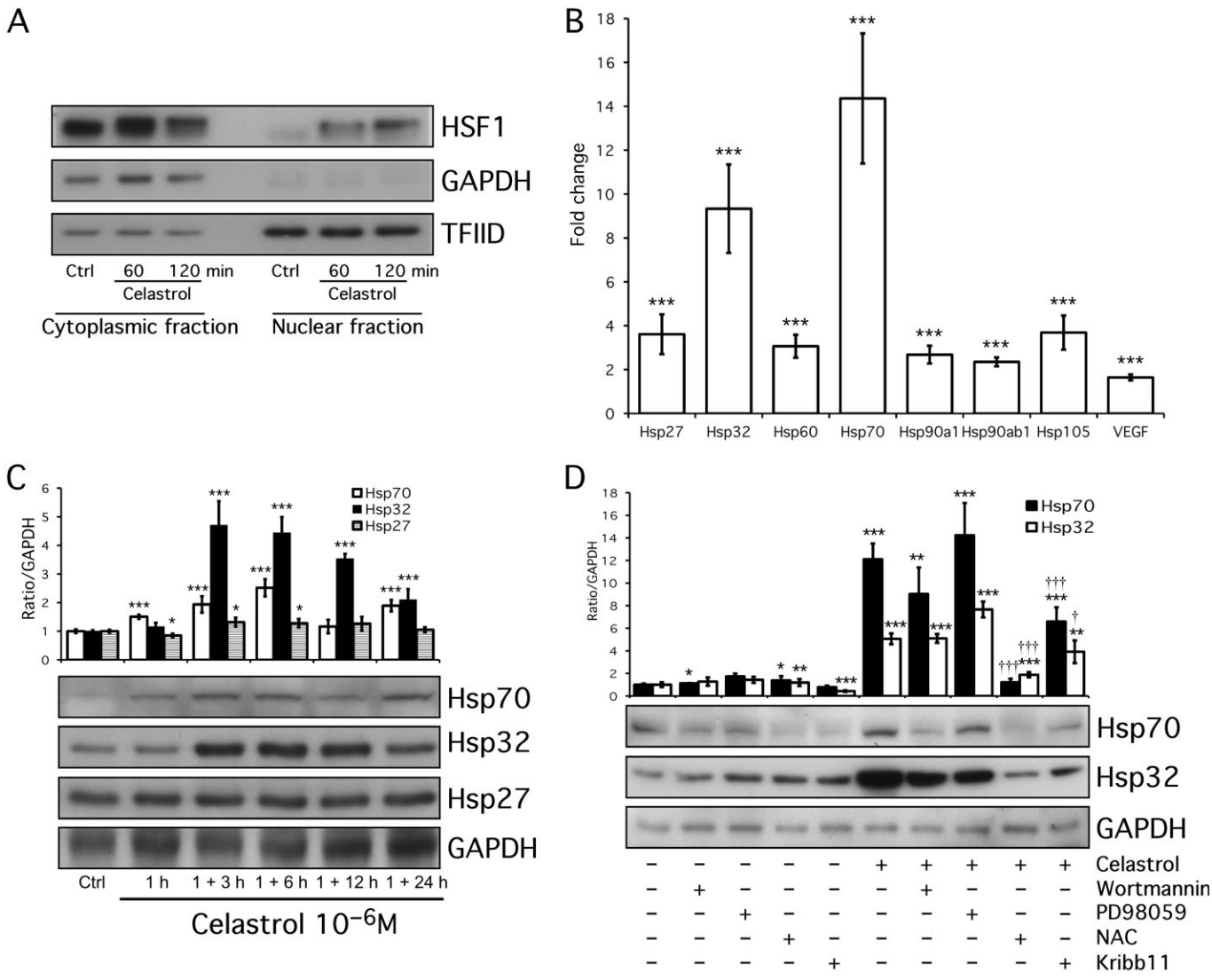

Figure 2

HSR induced by celastrol in H9c2 cells leading to up-regulation of HSPs is dependent on HSF1 and ROS signalling. (A) Treatment of H9c2 cells *in vitro* resulted in the nuclear translocation of the transcription factor HSF1. Representative Western blots for HSF1, GAPDH and transcription factor II D (housekeeping genes in cytoplasmic and nuclear fractions, respectively) following 10^{-6} M Celastrol treatment for 60 and 120 min. (B) Real-time PCR quantifications of HSP27, HSP32 (HO-1), HSP60, HSP70, HSP90a1 (HSP90α), HSP90ab1 (HSP90β), HSP105 and VEGF mRNA expression in H9c2 treated with 10^{-6} M celastrol for 60 min followed by 3 h washout. CT values were normalized on 18S and results analysed by Pfaffl method (primer sequences in Supporting Information). (C) Representative Western blot and quantification of HSP70, HSP32 and HSP27 proteins in H9c2 cultures after treatment with 10^{-6} M celastrol for 60 min followed by 0, 3, 6, 12 and 24 h washout period. (D) Representative Western blot of HSP32 (HO-1) and HSP70 proteins following treatment with 10^{-6} M celastrol for 60 min followed by 3 h washout. Celastrol up-regulation of HSPs expression was blocked by HSF1 inhibitor (Kribb11) and ROS scavenger (NAC), but not PI3K/AkT (wortmannin) or ERK1/2 (PD98059) pathway inhibitors. *$P < 0.05$, **$P < 0.01$ and ***$P < 0.001$ versus control or vehicle respectively. †$P < 0.05$ and †††$P < 0.001$ versus celastrol in celastrol-treated cells.

infiltration (Figure 5E). TGF-β3, a key factor for fibroblast differentiation into myofibroblasts, and collagen I and collagen III mRNA, products from myofibroblasts involved in tissue fibrosis, were significantly increased 2.4-, 2.3-, and 2.5-fold, respectively, in the ischaemia border zone compared with the non-ischaemic remote viable zone in control-treated rats (all $P < 0.05$, Figure 5F). Celastrol attenuated this increase in TGF-β3 and collagen I expression in the ischaemia border versus remote non-ischaemic zone, and the increased collagen III content in the ischaemia border zone was, however, significantly reduced with celastrol compared with control-treated rats (Figure 5F).

Taking into consideration fibrosis, scar tissue formation, inflammation, macrophage and myofibroblast infiltration, a comprehensive histological examination using a global damage index revealed that celastrol prevented adverse cardiac remodelling (Figure 6A–D). Similarly, celastrol treatment significantly reduced macrophage infiltration in the

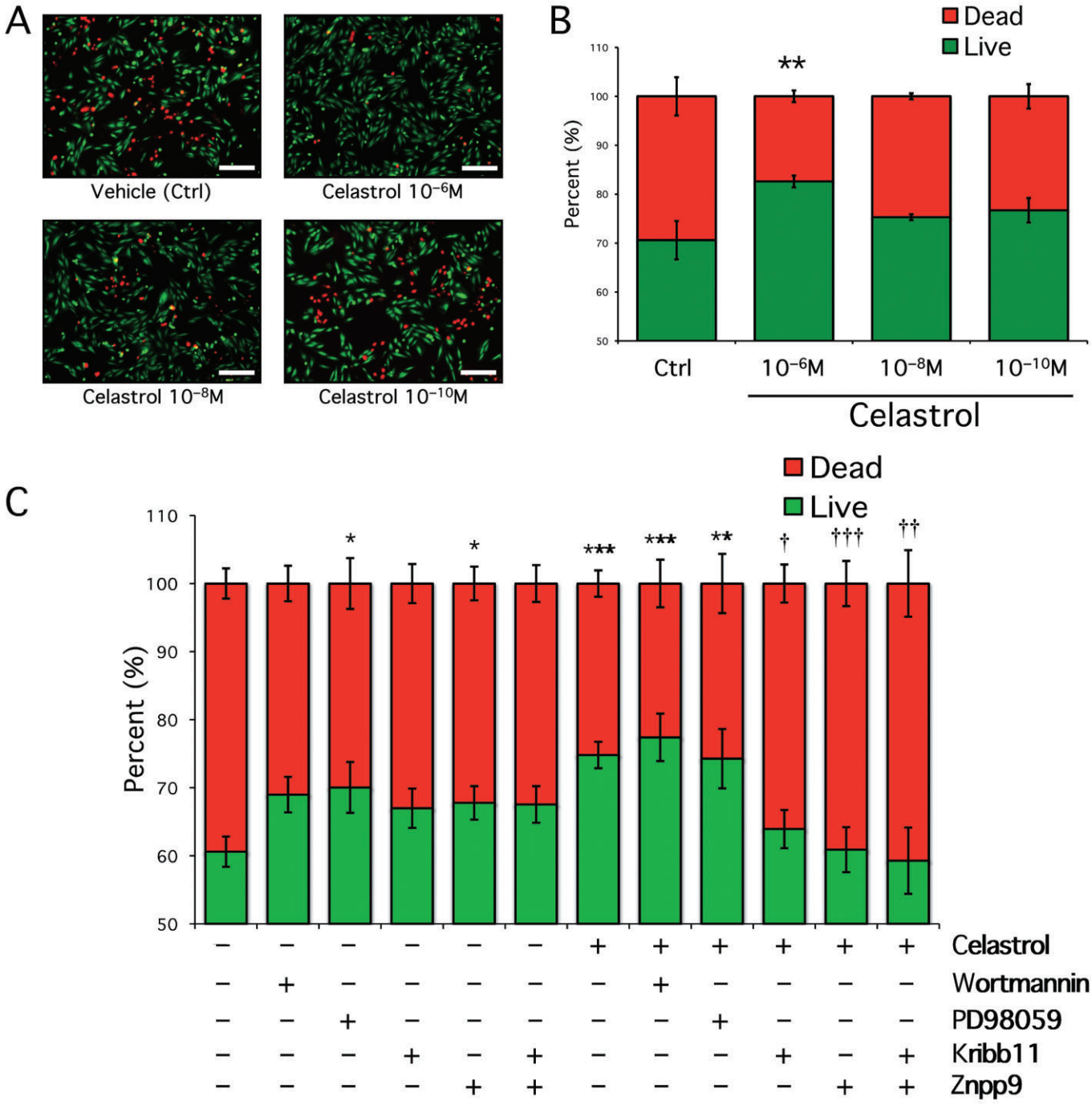

Figure 3

Celastrol protects H9c2 cell cultures from hypoxia-induced cell death *in vitro* through HSF1 and HO-1 mechanisms. (A) Representative fluorescent images of live/dead viability assay in vehicle- or celastrol-treated H9c2 cells and incubation in hypoxic conditions for 48 h. Living cells are green and dead cells are red. Scale bar = 0.25 mm. (B) H9c2 cells were treated for 1 h with vehicle (controls) or celastrol (10^{-10} to 10^{-6} M) followed by culture in low-serum, low-glucose hypoxic conditions (<1% O_2) for 48 h. Live/dead viability assay was performed on cultures, and results are expressed as percentages of alive and dead cells. (C) H9c2 cells were pretreated for 1 h with vehicle or 10^{-6} M celastrol in the presence of, or without, pathway inhibitors wortmannin, PD98059, Kribb11, ZnPP-9, Kribb11 + ZnPP-9, followed by culture in low-serum, low-glucose, hypoxic conditions (<1% O_2), and low-dose pathway inhibitors or Vehicle for 48 h. Live/dead viability assay was performed on cultures, and results are expressed as percentages of alive and dead cells. *P < 0.05, **P < 0.01 and ***P < 0.001 versus control condition. †P < 0.05, ††P < 0.01 and †††P < 0.001 versus celastrol in celastrol-treated cells.

Table 1

Echocardiography parameters of rat hearts at baseline and following MI or sham surgery and treated with celastrol or vehicle for 14 days

	Control sham (n = 6)		Treated sham (n = 7)		Control ischaemia (n = 10)		Treated ischaemia (n = 8)	
	Baseline	Day 14	Baseline	Day 14	Baseline	Day 14	Baseline	Day 14
LVEF (%)	83.8 ± 1.6	79.6 ± 1.7	84.4 ± 2.1	82.8 ± 1.6	84.6 ± 0.7	48.1 ± 4.5***,†	85.3 ± 0.9	65.6 ± 5.6***
LVFS (%)	53.8 ± 1.6	49.3 ± 1.8	54.5 ± 2.3	52.9 ± 1.7	54.3 ± 0.8	25.9 ± 2.9 ***,†	55.2 ± 1.0	38.3 ± 4.0***
LVAW (mm)	1.34 ± 0.04	1.53 ± 0.05***	1.31 ± 0.01	1.50 ± 0.14	1.39 ± 0.05	1.04 ± 0.19**	1.39 ± 0.04	1.33 ± 0.09
EDD (mm)	5.97 ± 0.18	6.42 ± 0.15	5.58 ± 0.15	5.79 ± 0.16	5.49 ± 0.12	7.93 ± 0.27***	5.42 ± 0.11	6.90 ± 0.37***
ESD (mm)	2.77 ± 0.17	3.25 ± 0.17	2.54 ± 0.15	2.75 ± 0.17	2.51 ± 0.07	5.93 ± 0.38***,†	2.43 ± 0.09	4.35 ± 0.50***

*P < 0.05, **P < 0.01 and ***P < 0.001 versus respective baseline conditions. †P < 0.05: δ (baseline, day 14) control versus δ (baseline, day 14) treated ischaemia.

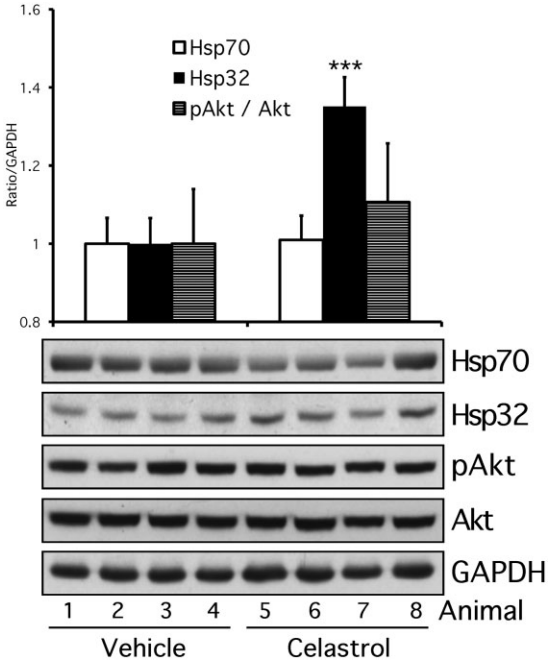

Figure 4

In vivo celastrol injection induces HO-1 expression in the rat heart. Densitometric quantification of HSP70, HSP32 (HO-1) and phosphorylated Akt (pAkt)/total Akt protein expressions corresponding to representative Western blot (n = 8 represented) in the rat heart at 12 h after single i.p. injection of vehicle (n = 8) or celastrol (1 mg·kg^{-1}) (n = 8). ***P < 0.0001 versus control.

peri-infarcted area by 3.97-fold versus control treatment, suggesting modulation of the inflammatory response following the reduced infarct size (75.1 ± 9.9 vs. 18.9 ± 4.4 macrophages per field, P < 0.001) (Figure 7A,B).

Celastrol improves functional recovery of infarcted heart

Echocardiography parameters were analysed according to baseline value and intergroup δ (baseline – day 14) comparisons as described (Nguyen *et al.*, 2010; Aceros *et al.*, 2011). At 2 weeks, echocardiography analysis demonstrated that sham procedure has no effect on LV cardiac function compared with baseline as presented by LVEF (%) and LVFS (%) (Table 1). Coronary artery ligation produced a large infarct that significantly reduced LVEF (%) and LVFS (%) in control ischaemia and celastrol-treated ischaemia animals (P < 0.001 vs. baseline). Celastrol treatment significantly improved cardiac functional recovery following MI with enhanced LVEF (%) and LVFS (%) compared with control ischaemia animals (P = 0.017 and P = 0.016 respectively). Compared with baseline, the large MI resulted in a significant thinning of LVAW in the control ischaemia animals (P = 0.004), which was not observed in the celastrol-treated animals (P = 0.443). Similarly, MI resulted in a significant LV dilatation at 2 weeks compared with baseline in both control and celastrol-treated ischaemia animals (all P < 0.001). However, celastrol treatment significantly prevented ESD deterioration (P = 0.0193), but attenuated EDD at 2 weeks (P = 0.059) (Table 1).

Discussion and conclusion

To our knowledge, the present study provides the first evidence that celastrol confers cardioprotection against ischaemic injury both *in vitro* and in an animal model of MI *in vivo*. Treatment of rat H9c2 cardiomyoblasts with celastrol induced a rapid ROS production as early as 5 min after exposure, and treatment with the free radical scavenger NAC inhibited Akt and ERK phosphorylation, suggesting that activation of these pathways are dependent on ROS signalling. Indeed, ROS in low concentrations serve as signalling molecules in ischaemic conditioning (Sun, 2009) in a mechanism referred to as 'redox or ROS signalling' (Sorescu and Griendling, 2002), and known to trigger activation of PKs (Daiber, 2010). Celastrol prompted the nuclear translocation of the transcription factor HSF1, resulting in a HSR through increased expression of cytoprotective HSPs detected both at the mRNA and protein level with maximal increase detected for HSP70 and HSP32 (HO-1). HSP32 or HO-1 is part of a protective mechanism expressed in response to various stimuli that are associated with oxidative stress and inflammation, and evidence points to HO-1 as one of the most important cardioprotective proteins (Dawn and Bolli, 2005). NAC and Kribb11 inhibitor

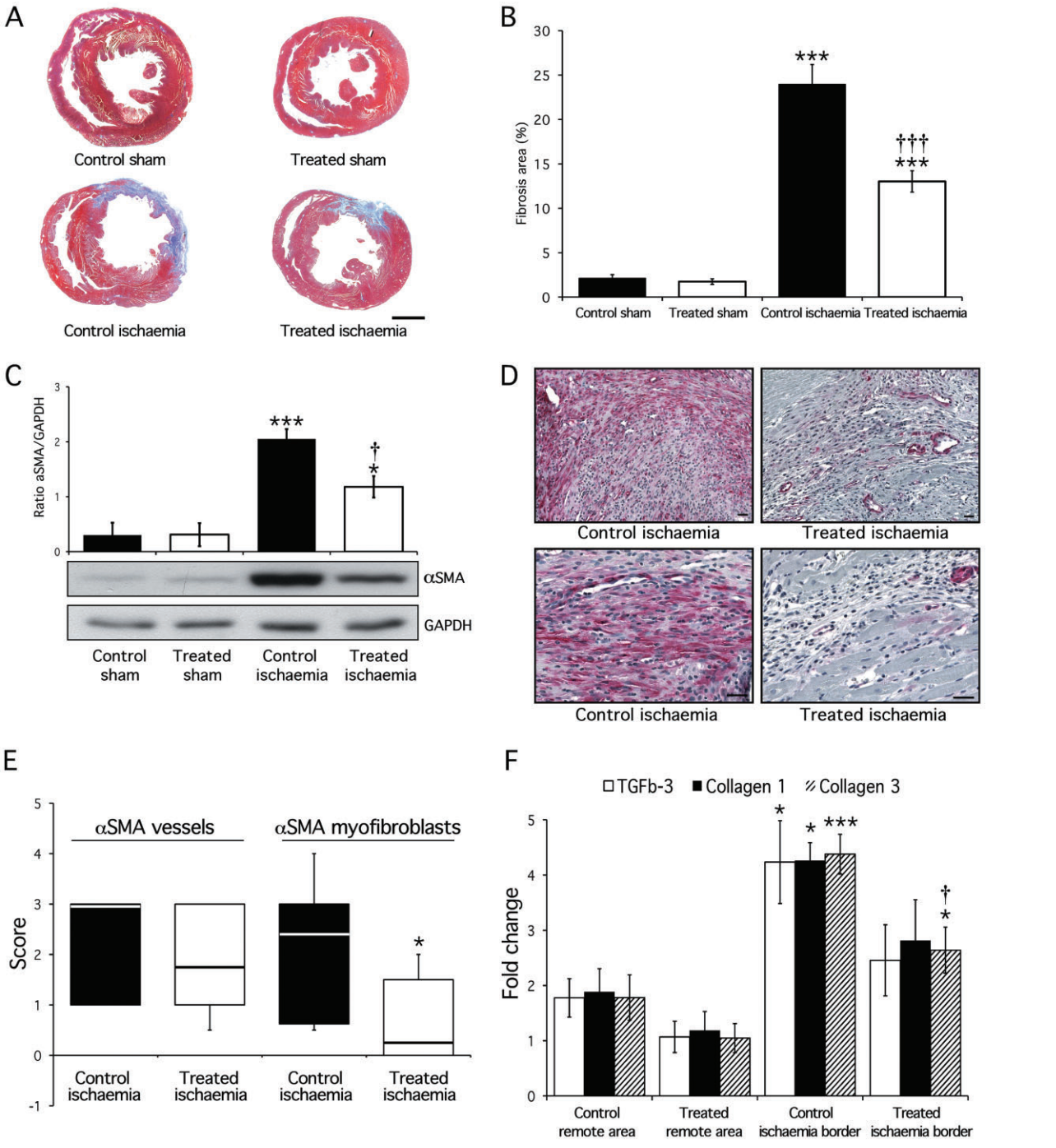

Figure 5

Celastrol reduces infarct size, αSMA deposition by myofibroblasts, and reduces up-regulation of TGF-β3, collagen I and III genes in the ischaemic infarct border zone at 14 days. (A) Representative digitalized pictures of Masson's trichrome-stained ventricular sections after 2 weeks, where blue areas indicate fibrotic infarcted myocardium. Scale bar = 0.25 cm. (B) Planimetric quantifications of fibrosis (blue areas stained by Masson's trichrome over total LV area in percentage) demonstrated a reduction of the infarcted area in the celastrol-treated animals. (C) Histogram of densitometric quantification of αSMA protein expressions in viable and infarct border zone with corresponding representative Western blot. (D) Representative immunohistological staining to detect αSMA in infarct border zone demonstrating important tissue infiltration by myofibroblasts (red) in Control animals compared with celastrol-treated animals. Scale bar = 0.025 mm. (E) Score provided separately for immunohistological staining of αSMA accounting for blood vessels and myofibroblast demonstrated that celastrol significantly reduced myofibroblast infiltration in infarcted tissue. Data expressed as box plot for quartile range and median representation, and whiskers identifying smallest and largest values. (F) Real-time PCR expression of TGF-β3, collagen I and III mRNA in the non-ischaemic remote and infarcted border area for vehicle and celastrol-treated animals. *$P < 0.05$, ***$P < 0.001$ versus sham animals or non-ischaemic remote areas, respectively. †$P < 0.05$, †††$P < 0.001$ versus control treatment in ischaemia animals or ischaemia border area in control-treated animals.

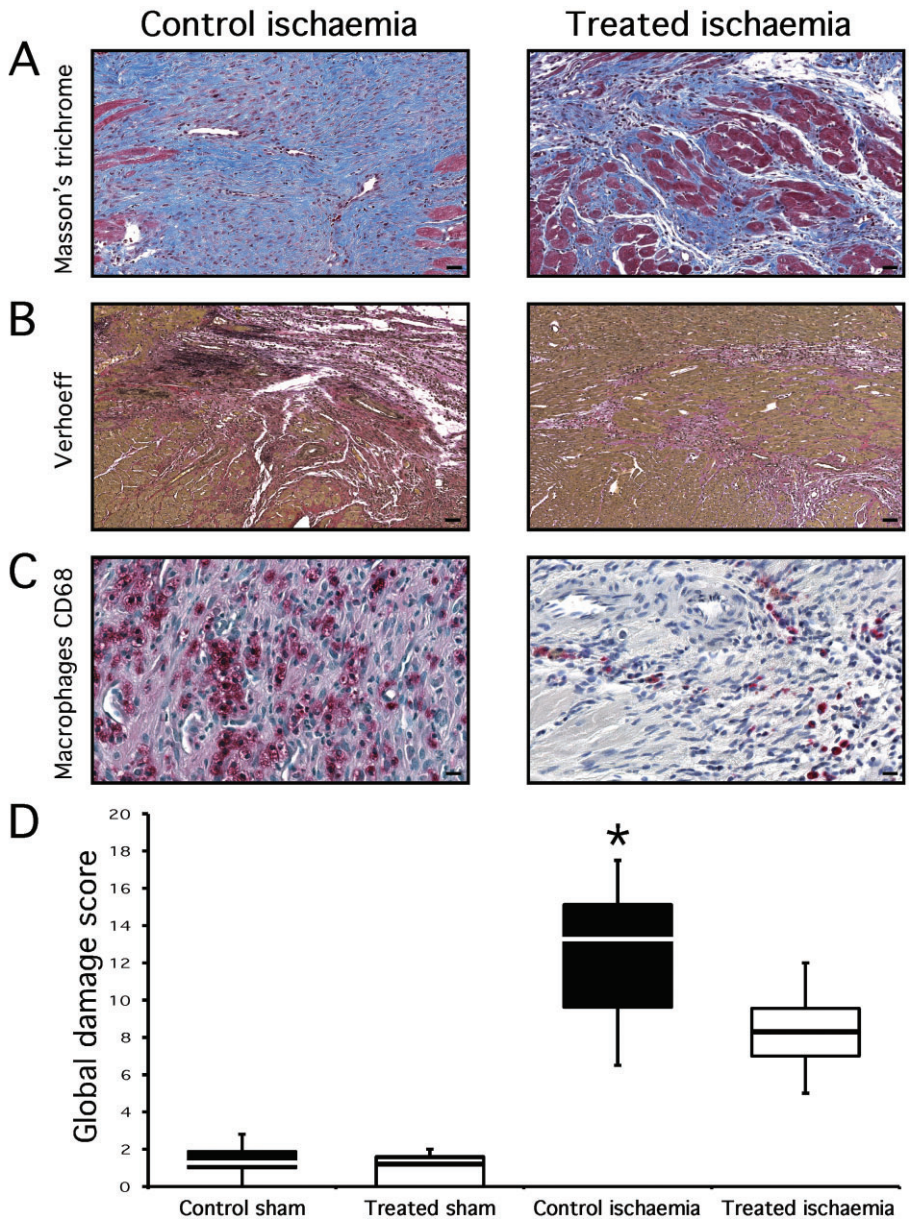

Figure 6

Celastrol reduces global tissue damage in the infarcted myocardium at 14 days. Representative pictures of histological sections of infarct area of rats treated with control or celastrol (1 mg·kg^{-1}) for 2 weeks. Sections are stained with (A) Masson's trichrome, scale bar = 0.025 mm; (B) Verhoeff stain, scale bar = 0.05 mm; (C) Anti-CD68 macrophage antibody (ED1), scale bar = 0.01 mm; (D) Histogram representing global tissue damage index developed by the compilation of scoring of 1-αSMA vessels and tissue, 2-Masson's trichrome, 3-Verhoeff and 4 macrophages staining on a scale of 0 (absent) to 4 (high) of parameters the parameters mentioned earlier by an expert pathologist unaware of the experimental groups. Data expressed as box plot for quartile range and median representation, and whiskers identifying smallest and largest values. *$P < 0.05$ versus respective sham animals.

significantly reduced HSP overexpression, providing evidence that both ROS and HSF1 are important mediators of the celastrol-induced HSR leading to HO-1 signalling. Similar to our data, Seo *et al*. recently showed that celastrol-induced expression of HO-1 was mediated by ROS signalling in human keratinocytes (Seo *et al*., 2011).

Celastrol treatment of H9c2 exposed to hypoxic and serum starvation conditions mimicking the MI environment dose-dependently reduced cell death. Importantly, functional analysis with inhibitors revealed the importance of HSF1 and HO-1, but not PI3K/AkT and ERK1/2 pathways, as key effectors of the cytoprotective HSR induced by celastrol. Interestingly, increased expression of HO-1 with a 1 h celastrol treatment observed in our study was further elevated when cultures were submitted to hypoxia until 24 h (not shown), which suggests the effectiveness of celastrol in sensitizing and

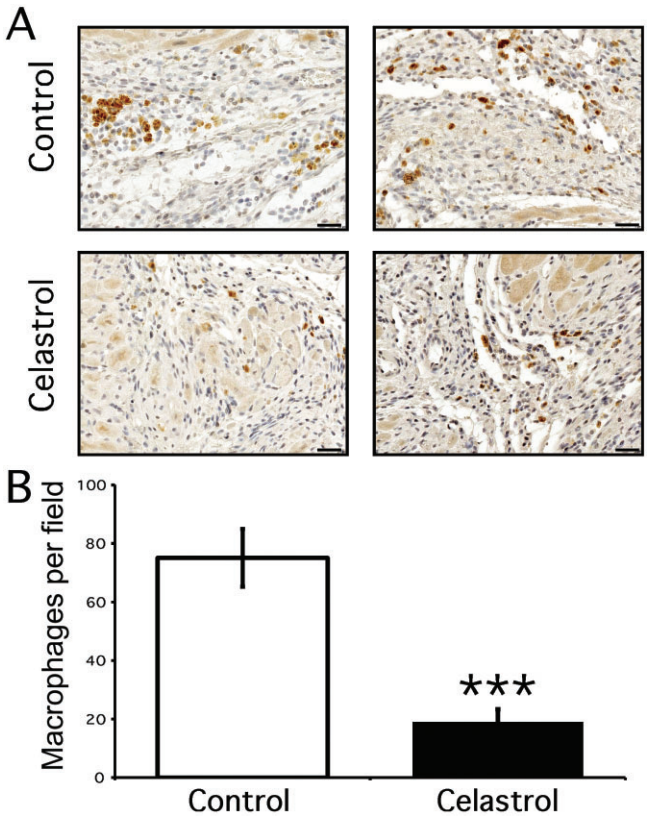

Figure 7

Celastrol reduces macrophage infiltration in the infarcted myocardium at 14 days. (A) Representative histological sections of infarct area of four different rats treated with control or celastrol (1 mg·kg^{-1}) for 2 weeks. Sections are stained with F4/80 macrophage antibody. Scale bar = 0.03 mm. (B) Histogram of macrophage infiltration in the infarct area. For each rat, all macrophages in five randomly chosen pictures in the infarct area were counted and results were averaged and expressed as macrophages per sampling field. ***P < 0.001 versus control.

sustaining a therapeutic effect in cells exposed to hypoxic condition. This said, as ERK1/2 and Akt/PI3K pathways are recognized as transducers of anti-apoptotic signals and involved in the early phase of ischaemic conditioning, it is possible that the *in vitro* experimental model of continuous hypoxic stress in low-glucose environment without reoxygenation, could not highlight the importance of these pathways, as published by Liu *et al.* using an ischaemia/reperfusion model (Liu *et al.*, 2012). However, Hillion *et al.* reported that oxygen and glucose deprivation could transiently activate Akt, and pharmacological blockade of the PI3K/Akt pathway could induce ischaemia tolerance and reduce cell death (Hillion *et al.*, 2006). Also Hamilton *et al.* reported that inhibition of Akt and p38 MAPK activities led to decreased apoptosis compared with hypoxia alone (Hamilton *et al.*, 2012). Therefore, the role of Akt and ERK as mediators of anti-apoptotic signalling may be model- and/or cell type-dependent, and may be only marginal in our observed findings, with cell survival largely dependent on the up-regulation of HO-1 expression through ROS and HSF1 signalling.

In the rat heart, up-regulation of HO-1 was demonstrated 12 h after *in vivo* celastrol treatment of non-infarcted rats, confirming the mechanism observed with *in vitro* experiments at the whole organ level. Interestingly, overexpression of the cardioprotective protein HO-1 was also detected in the plasma of celastrol-treated rats, suggesting systemic response and possible beneficial effects on various organs. Administration of celastrol initiated immediately after the onset of MI was effective in improving cardiac function, and preventing anterior wall thinning and LV enlargement. Moreover, celastrol reduced infarct size, myofibroblast infiltration, and macrophage influx. Immunohistological analyses revealed a clear dichotomic pattern between celastrol-treated and control animals. The global damage score, which takes into account late inflammation with CD68 (macrophage marker), scar tissue formation from αSMA, Masson's trichrome and Verhoeff's stainings, highlighted a striking reduction in overall score with celastrol treatment. Analysis of αSMA immunostaining demonstrated a clear reduction of myofibroblast infiltration in the celastrol treatment group, but no change in blood vessel formation in the ischaemic tissue.

TGF-β is the most important regulator of the fibrotic response after MI and modulates the proliferation, migration and differentiation of fibroblasts into myofibroblasts expressing *de novo* high level of αSMA. Activated myofibroblasts are responsible for the production and deposition of collagen types I and III (Grotendorst *et al.*, 2004), leading to the establishment of a dense extracellular matrix found in the healing and remodelling process following MI. In our experimental model, ischaemic injury increased TGF-β and collagen expression in ischaemic and remote areas, but celastrol attenuated TGF-β3 and collagen types I and III gene up-regulation in the infarcted border zone compared with non-ischaemic remote area. Together, our results tie in the reduced damage and fibrotic responses measured in the infarct border zone of celastrol-treated rats and suggest that following ischaemia, celastrol reduced cardiomyocyte loss, lead to improved cardiac wound healing, reduced early tissue damage and adverse myocardial remodelling.

Celastrol is recognized as one of the most promising medicinal molecules isolated from plant extracts (Salminen *et al.*, 2010) with beneficial effects in the treatment of different forms of neurodegenerative and autoimmune diseases, as well as inflammatory conditions (Allison *et al.*, 2001; Pinna *et al.*, 2004). In a model of rat acute brain ischaemic injury, Li *et al.* demonstrated that a single i.p. injection of celastrol reduced neurological deficit and brain infarct size at 24 h (Li *et al.*, 2012). Yu *et al.* reported the beneficial effects of celastrol on myocytes size in hypertensive rats (Yu *et al.*, 2010), and Chu *et al.* (2014) demonstrated that celastrol reduced rat kidney ischaemia-reperfusion injury, which was associated with reduced local NF-κB activation, TNF, ILs and inflammation. Similar to our observations, Chow *et al.* demonstrated that, as opposed to classical heat shock treatment, 10^{-6} M celastrol induced HSP27, HO-1 and HSP70 in mature brain cortical cultures (Chow *et al.*, 2012), and reduced *in vivo* neuropathological features of Alzheimer's disease (Paris *et al.*, 2010). Finally, the pharmacokinetic properties of celastrol in rats have been published (Wang *et al.*, 2008; Zhang *et al.*, 2012), and systemic administration of 1 mg·kg^{-1} dose provided a plasma concentration of 0.05 μg·mL^{-1} (0.1 μM

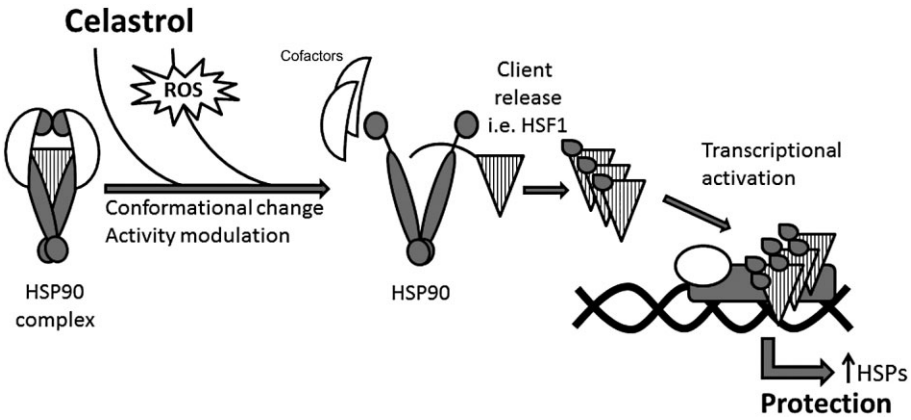

Figure 8

Proposed mechanism of celastrol actions. HSP90 ensures the proper folding, maturation, stability and activation of many important 'client' proteins including PKs such as Akt, ERK and transcription factors including HSF1 and HIF1. By interacting with HSP90 complex and essential cofactors (i.e. Cdc37, p23), and/or indirectly through the generation of ROS with disruption of HSP90 complex or solicitation of HSP90 in the maintenance of protein homeostasis, celastrol promotes dissociation of client proteins from HSP90. The cytoplasmic release of proteins with short burst treatment lead to the activation of multiple pathways involved in cell survival and cytoprotection akin to protocols of transient genomic overexpression. In this example, HSF1 monomer is bound to HSP90, and upon exposure to celastrol, HSF1 dissociates and translocates into the nucleus where it binds as a trimer to HSR elements in gene promoters and drives transcriptional activation of HSPs leading to cytoprotection.

equivalent) with excellent linearity over several hours. Interestingly, the mg·kg^{-1} *in vivo* dose used in the present study is also in range with the optimal dose for *in vitro* viability of <1 μM used in our experiments and published by others (Hansen *et al.*, 2011).

Celastrol, is considered a modulator of the activity of HSP90, which is one of the most abundant proteins in the cytoplasm playing an essential role in many cellular processes and signalling pathways (Jackson, 2013). HSP90 is required for maturation and activation of a number of key cellular proteins, called 'clients', enabling their appropriate folding, stabilization, transportation and even degradation. The number of identified HSP90 clients has increased dramatically in recent years and the list contains most importantly kinases and transcription factors, including Akt, MAPK and HSF1, many of which are important in controlling cell growth, proliferation, differentiation and survival (Taipale *et al.*, 2010). Under 'normal' conditions, HSF1, the key regulator of HSR, exists in a repressed non-trimeric state associated with its chaperon inhibitor HSP90 (Westerheide *et al.*, 2004). Upon stress or activation, HSF1 undergoes relocalization in the nucleus, and binds to heat shock promoter elements resulting in the coordinated elevated transcription of cytoprotective HSPs.

Earlier studies from other groups, together with our findings, suggested that the conditioning pathways activated by celastrol may be explained by its ability to modulate HSP90 activity. In fact, celastrol was shown to disrupt HSP90 and essential cofactor complex detrimental to HSP90's activity (Zhang *et al.*, 2008; 2009; Sreeramulu *et al.*, 2009; Chadli *et al.*, 2010), thereby modifying the activity and signalling of its client proteins. The induction of disruptive conformational change induced by HSP90 inhibitors will provoke the release of client proteins that will eventually be degraded (Blagg and Kerr, 2006). Moreover, our findings, in line with others, showed that celastrol increased ROS formation (Chen *et al.*, 2011). This may disrupt the HSP90 chaperone activity (Sarkar *et al.*, 2013) and/or solicit HSP90 in the maintenance of protein homeostasis resulting with HSP90 competing between protein stabilization and its client proteins. The latter being released in the cytoplasm may further participate to intracellular signalling processes. Overall, celastrol may activate signalling pathways similar to ischaemic/thermal conditioning by direct mechanisms involving conformational changes of HSP90 complex and/or indirect mechanism by generation of ROS, which will result in the release of clients from HSP90 complex and trigger survival signalling pathways leading to a HSR (Figure 8).

In conclusion, this study provides evidence that celastrol exerts a cardioprotective effect in the context of MI, and may act as an infarct-sparing pharmacological agent. Our studies with cardiomyoblasts show that celastrol can mimic ischaemic/thermal conditioning and promote cell survival through activation of HSF1 with up-regulation of HO-1 as key effector in cellular survival. Celastrol's efficacy in reducing early cardiac injury could benefit the repair process, and thereby represent a new treatment perspective for patients suffering from ischaemic heart disease.

Limitations

As a surrogate for primary cells, we used the H9c2 rat cardiomyoblast cell line, which have the advantage of being a well-characterized and validated model mimicking primary cardiomyocytes *in vitro* (Zordoky and El-Kadi, 2007; Watkins *et al.*, 2011). H9c2 cells are extensively used for investigating myocardial damage and cardiomyopathies, and using a similar approach to ours, Sun *et al.* recently reported the effects of ginsenoside in ischaemia/reperfusion-induced apoptosis in H9c2 cells with extensive investigation of signalling pathways (Sun *et al.*, 2013). Celastrol was injected within 3 h

post-infarction, which would be suitable for the human applicability in the clinical setting of an acute MI without reperfusion, thus presenting celastrol as a valuable treatment for ischaemic post-conditioning for cases of reperfusion therapy failure. Of note, the *in vivo* study validated our *in vitro* findings using cultured H9c2 cardiomyoblasts without reoxygenation. It would be interesting to speculate similar beneficial effect of celastrol in the myocardial ischaemia/reperfusion model.

Acknowledgements

This work was supported by the Heart and Stroke Foundation of Canada, Pfizer Cardiovascular Research Award, Cell Therapy Translational Research Platform FRQS-HMR, FRQS/ThéCell and the Department of Surgery of the Université de Montréal. J.-F. C., L.-M. S., S. M. and N. N. are scholars of FRQ-S. J.-F. C. holds the Chair Claude-Bertrand in Neurosurgery of the University of Montreal. The authors wish to thank Dr Ewa Wesolowska and Dr Marc Martin at the Clinical Biochemistry Department of the CHUM Hôtel-Dieu Hospital for biochemical assays and helpful discussions.

Author contributions

All authors have read and approved the submission of the paper. S. D. Sarkissian. did the study concept and experimental design, wrote the paper, did the ROS and viability studies, and did data analysis. J.-F. C. did the macrophage studies, characterization of the inflammation and the figures. M. B. did the gene and protein expression and viability studies, and the figures. L.-M. S. did statistical analysis. L. G. did histopathology comprehensive studies and evaluation of cardiac remodelling. S. M. did the study concept and data analysis. P. H. did the study concept, chose the animal and the experimental models. N. N. did the study concept and experimental design, animal surgery, wrote the paper and did the figures, planimetry, data analysis, and is the corresponding author.

Conflict of interest

None declared.

References

Aceros H, Farah G, Cobos-Puc L, Stabile AM, Noiseux N, Mukaddam-Daher S (2011). Moxonidine improves cardiac structure and performance in SHR through inhibition of cytokines, p38 MAPK and Akt. Br J Pharmacol 164: 946–957.

Alexander SPH, Benson HE, Faccenda E, Pawson AJ, Sharman JL, Spedding M *et al.* (2013). The Concise Guide to PHARMACOLOGY 2013/14: Enzymes. British Journal of Pharmacology, 170: 1797–1867.

Allison AC, Cacabelos R, Lombardi VR, Alvarez XA, Vigo C (2001). Celastrol, a potent antioxidant and anti-inflammatory drug, as a possible treatment for Alzheimer's disease. Prog Neuropsychopharmacol Biol Psychiatry 25: 1341–1357.

Blagg BS, Kerr TD (2006). Hsp90 inhibitors: small molecules that transform the Hsp90 protein folding machinery into a catalyst for protein degradation. Med Res Rev 26: 310–338.

Chadli A, Felts SJ, Wang Q, Sullivan WP, Botuyan MV, Fauq A *et al.* (2010). Celastrol inhibits Hsp90 chaperoning of steroid receptors by inducing fibrillization of the Co-chaperone p23. J Biol Chem 285: 4224–4231.

Chen G, Zhang X, Zhao M, Wang Y, Cheng X, Wang D *et al.* (2011). Celastrol targets mitochondrial respiratory chain complex I to induce reactive oxygen species-dependent cytotoxicity in tumor cells. BMC Cancer 11: 170.

Chow AM, Tang DW, Hanif A, Brown IR (2012). Induction of heat shock proteins in cerebral cortical cultures by celastrol. Cell Stress Chaperones 18: 155–160.

Chu C, He W, Kuang Y, Ren K, Gou X (2014). Celastrol protects kidney against ischemia-reperfusion-induced injury in rats. J Surg Res 186: 398–407.

Daiber A (2010). Redox signaling (cross-talk) from and to mitochondria involves mitochondrial pores and reactive oxygen species. Biochim Biophys Acta 1797: 897–906.

Dawn B, Bolli R (2005). HO-1 induction by HIF-1: a new mechanism for delayed cardioprotection? Am J Physiol Heart Circ Physiol 289: H522–H524.

Der Sarkissian S, Grobe JL, Yuan L, Narielwala DR, Walter GA, Katovich MJ *et al.* (2008). Cardiac overexpression of angiotensin converting enzyme 2 protects the heart from ischemia-induced pathophysiology. Hypertension 51: 712–718.

Finegold JA, Asaria P, Francis DP (2013). Mortality from ischaemic heart disease by country, region, and age: statistics from World Health Organisation and United Nations. Int J Cardiol 168: 934–945.

Grotendorst GR, Rahmanie H, Duncan MR (2004). Combinatorial signaling pathways determine fibroblast proliferation and myofibroblast differentiation. FASEB J 18: 469–479.

Haider H, Ashraf M (2008). Strategies to promote donor cell survival: combining preconditioning approach with stem cell transplantation. J Mol Cell Cardiol 45: 554–566.

Hamilton JA, Lacey DC, Turner A, de Kok B, Huynh J, Scholz GM (2012). Hypoxia enhances the proliferative response of macrophages to CSF-1 and their pro-survival response to TNF. PLoS ONE 7: e45853.

Hansen J, Palmfeldt J, Vang S, Corydon TJ, Gregersen N, Bross P (2011). Quantitative proteomics reveals cellular targets of celastrol. PLoS ONE 6.

Hillion JA, Li Y, Maric D, Takanohashi A, Klimanis D, Barker JL *et al.* (2006). Involvement of Akt in preconditioning-induced tolerance to ischemia in PC12 cells. J Cereb Blood Flow Metab 26: 1323–1331.

Jackson SE (2013). Hsp90: structure and function. Top Curr Chem 328: 155–240.

Kilkenny C, Browne W, Cuthill IC, Emerson M, Altman DG (2010). Animal research: reporting *in vivo* experiments: the ARRIVE guidelines. Br J Pharmacol 160: 1577–1579.

Laflamme MA, Zbinden S, Epstein SE, Murry CE (2007). Cell-based therapy for myocardial ischemia and infarction: pathophysiological mechanisms. Ann Rev Pathol 2: 307–339.

Li Y, He D, Zhang X, Liu Z, Zhang X, Dong L *et al*. (2012). Protective effect of celastrol in rat cerebral ischemia model: down-regulating p-JNK, p-c-Jun and NF-kappaB. Brain Res 1464: 8–13.

Liu SX, Zhang Y, Wang YF, Li XC, Xiang MX, Bian C *et al*. (2012). Upregulation of heme oxygenase-1 expression by hydroxysafflor yellow A conferring protection from anoxia/reoxygenation-induced apoptosis in H9c2 cardiomyocytes. Int J Cardiol 160: 95–101.

McGrath J, Drummond G, McLachlan E, Kilkenny C, Wainwright C (2010). Guidelines for reporting experiments involving animals: the ARRIVE guidelines. Br J Pharmacol 160: 1573–1576.

Murry CE, Jennings RB, Reimer KA (1991). New insights into potential mechanisms of ischemic preconditioning. Circulation 84: 442–445.

Nguyen BK, Maltais S, Perrault LP, Tanguay JF, Tardif JC, Stevens LM *et al*. (2010). Improved function and myocardial repair of infarcted heart by intracoronary injection of mesenchymal stem cell-derived growth factors. J Cardiovasc Transl Res 3: 547–558.

Noiseux N, Borie M, Desnoyers A, Menaouar A, Stevens LM, Mansour S *et al*. (2012). Preconditioning of stem cells by oxytocin to improve their therapeutic potential. Endocrinology 153: 5361–5372.

Noiseux N, Gnecchi M, Lopez-Ilasaca M, Zhang L, Solomon SD, Deb A *et al*. (2006). Mesenchymal stem cells overexpressing Akt dramatically repair infarcted myocardium and improve cardiac function despite infrequent cellular fusion or differentiation. Mol Ther 14: 840–850.

Ovize M, Thibault H, Przyklenk K (2013). Myocardial conditioning: opportunities for clinical translation. Circ Res 113: 439–450.

Paris D, Ganey NJ, Laporte V, Patel NS, Beaulieu-Abdelahad D, Bachmeier C *et al*. (2010). Reduction of beta-amyloid pathology by celastrol in a transgenic mouse model of Alzheimer's disease. J Neuroinflammation 7: 17.

Pawson AJ, Sharman JL, Benson HE, Faccenda E, Alexander SP, Buneman OP *et al*.; NC-IUPHAR (2014). The IUPHAR/BPS Guide to PHARMACOLOGY: an expert-driven knowledge base of drug targets and their ligands. Nucl. Acids Res. 42 (Database Issue): D1098–1106.

Pfaffl MW (2001). A new mathematical model for relative quantification in real-time RT-PCR. Nucleic Acids Res 29: e45.

Pinna GF, Fiorucci M, Reimund JM, Taquet N, Arondel Y, Muller CD (2004). Celastrol inhibits pro-inflammatory cytokine secretion in Crohn's disease biopsies. Biochem Biophys Res Commun 322: 778–786.

Salminen A, Lehtonen M, Paimela T, Kaarniranta K (2010). Celastrol: molecular targets of thunder god vine. Biochem Biophys Res Commun 394: 439–442.

Santiago JJ, Dangerfield AL, Rattan SG, Bathe KL, Cunnington RH, Raizman JE *et al*. (2010). Cardiac fibroblast to myofibroblast differentiation *in vivo* and *in vitro*: expression of focal adhesion components in neonatal and adult rat ventricular myofibroblasts. Dev Dyn 239: 1573–1584.

Sarkar S, Dutta D, Samanta SK, Bhattacharya K, Pal BC, Li J *et al*. (2013). Oxidative inhibition of Hsp90 disrupts the super-chaperone complex and attenuates pancreatic adenocarcinoma *in vitro* and *in vivo*. Int J cancer 132: 695–706.

Schett G, Steiner CW, Groger M, Winkler S, Graninger W, Smolen J *et al*. (1999). Activation of Fas inhibits heat-induced activation of HSF1 and up-regulation of hsp70. FASEB J 13: 833–842.

Seo WY, Goh AR, Ju SM, Song HY, Kwon DJ, Jun JG *et al*. (2011). Celastrol induces expression of heme oxygenase-1 through ROS/Nrf2/ARE signaling in the HaCaT cells. Biochem Biophys Res Commun 407: 535–540.

Solomon SD, Anavekar N, Skali H, McMurray JJ, Swedberg K, Yusuf S *et al*. (2005). Influence of ejection fraction on cardiovascular outcomes in a broad spectrum of heart failure patients. Circulation 112: 3738–3744.

Sorescu D, Griendling KK (2002). Reactive oxygen species, mitochondria, and NAD(P)H oxidases in the development and progression of heart failure. Congest Heart Fai 8: 132–140.

Sreeramulu S, Gande SL, Gobel M, Schwalbe H (2009). Molecular mechanism of inhibition of the human protein complex Hsp90-Cdc37, a kinome chaperone-cochaperone, by triterpene celastrol. Angew Chem Int Ed Engl 48: 5853–5855.

Stabile AM, Aceros H, Stockmeyer K, Abdel Rahman AA, Noiseux N, Mukaddam-Daher S (2011). Functional and molecular effects of imidazoline receptor activation in heart failure. Life Sci 88: 493–503.

Sun J, Sun G, Meng X, Wang H, Wang M, Qin M *et al*. (2013). Ginsenoside RK3 prevents hypoxia-reoxygenation induced apoptosis in H9c2 cardiomyocytes via AKT and MAPK pathway. Evid Based Complement Alternat Med 2013: 690190.

Sun Y (2009). Myocardial repair/remodelling following infarction: roles of local factors. Cardiovasc Res 81: 482–490.

Taipale M, Jarosz DF, Lindquist S (2010). HSP90 at the hub of protein homeostasis: emerging mechanistic insights. Nat Rev Mol Cell Biol 11: 515–528.

Wang W, Liu K, Dong H, Liu W (2008). High-performance liquid chromatography spectrometric analysis of tripterin in rat plasma. J Chromatogr B Analyt Technol Biomed Life Sci 863: 163–166.

Watkins SJ, Borthwick GM, Arthur HM (2011). The H9C2 cell line and primary neonatal cardiomyocyte cells show similar hypertrophic responses *in vitro*. In Vitro Cell Dev Biol Anim 47: 125–131.

Westerheide SD, Bosman JD, Mbadugha BN, Kawahara TL, Matsumoto G, Kim S *et al*. (2004). Celastrols as inducers of the heat shock response and cytoprotection. J Biol Chem 279: 56053–56060.

Yoon YJ, Kim JA, Shin KD, Shin DS, Han YM, Lee YJ *et al*. (2011). KRIBB11 inhibits HSP70 synthesis through inhibition of heat shock factor 1 function by impairing the recruitment of positive transcription elongation factor b to the hsp70 promoter. J Biol Chem 286: 1737–1747.

Yu X, Tao W, Jiang F, Li C, Lin J, Liu C (2010). Celastrol attenuates hypertension-induced inflammation and oxidative stress in vascular smooth muscle cells via induction of heme oxygenase-1. Am J Hypertens 23: 895–903.

Zhang J, Li CY, Xu MJ, Wu T, Chu JH, Liu SJ *et al*. (2012). Oral bioavailability and gender-related pharmacokinetics of celastrol following administration of pure celastrol and its related tablets in rats. J Ethnopharmacol 144: 195–200.

Zhang T, Hamza A, Cao X, Wang B, Yu S, Zhan CG *et al*. (2008). A novel Hsp90 inhibitor to disrupt Hsp90/Cdc37 complex against pancreatic cancer cells. Mol Cancer Ther 7: 162–170.

Zhang T, Li Y, Yu Y, Zou P, Jiang Y, Sun D (2009). Characterization of celastrol to inhibit hsp90 and cdc37 interaction. J Biol Chem 284: 35381–35389.

Zordoky BN, El-Kadi AO (2007). H9c2 cell line is a valuable *in vitro* model to study the drug metabolizing enzymes in the heart. J Pharmacol Toxicol Methods 56: 317–322.

Supporting information

Additional Supporting Information may be found in the online version of this article at the publisher's web-site:

http://dx.doi.org/10.1111/bph.12838

Figure S1 Two weeks *in vivo* celastrol treatment shows no difference for general biochemistry markers monitoring liver, kidney and heart health. Celastrol (1 mg·kg^{-1} per day) was injected daily i.p. in rats for 2 weeks, and compared with saline (0.9% NaCl) or vehicle (DMSO) injections. Serum biochemistry showed no difference for general markers useful in monitoring liver, kidney and heart health. N = 3–4 animals per group. Repeated measures ANOVA and ANOVA followed by Bonferroni correction for each time point.

Table S1 Real-time PCR primer sequences.